Anomalously weak Labrador Sea convection and Atlantic overturning during the past 150 years

Article

Accepted Version

Thornalley, D. J. R., Oppo, D. W., Ortega, P., Robson, J., Brierley, C. M., Davis, R., Hall, I. R., Moffa-Sanchez, P., Rose, N. L., Spooner, P. T., Yashayaev, I. and Keigwin, L. D. (2018) Anomalously weak Labrador Sea convection and Atlantic overturning during the past 150 years. Nature, 556 (7700). pp. 227-230. ISSN 0028-0836 doi: https://doi.org/10.1038/s41586-018-0007-4 Available at http://centaur.reading.ac.uk/76608/

"Anomalously weak Labrador Sea convection and Atlantic overturning during the past 150 years"

David J.R. Thornalley[1,2*], Delia W. Oppo[2], Pablo Ortega[3], Jon I. Robson[3], Chris M. Brierley[1], Renee Davis[1], Ian R. Hall[4], Paola Moffa-Sanchez[4], Neil L. Rose[1], Peter T. Spooner[1], Igor Yashayaev[5] & Lloyd D. Keigwin[2]

1) University College London, Department of Geography, UK

2) Woods Hole Oceanographic Institution, Department of Geology and Geophysics, USA

3) University of Reading, Department of Meteorology, Reading, U.K.

4) Cardiff University, School of Earth and Ocean Sciences, UK

5) Fisheries and Oceans Canada, Bedford Institute of Oceanography, Dartmouth, Canada

*To whom correspondence should be sent d.thornalley@cantab.net

The Atlantic meridional overturning circulation (AMOC) plays an essential role in climate through its redistribution of heat and its influence on the carbon cycle[1,2]. A recent decline in the AMOC may reflect decadal variability in Labrador Sea convection, but short observational datasets preclude a longer-term perspective on the modern state and variability of Labrador Sea convection and AMOC[1,3-5]. Here, we provide several lines of paleoceanographic evidence that Labrador Sea deep convection and AMOC have been anomalously weak over the past ~150 years (since the end of the Little Ice Age, LIA; ~1850 CE), in comparison to the preceding ~1500 years. The reconstructions suggest the transition occurred as an abrupt shift around the end of the LIA, or, a more gradual, continued decline over the past 150 years; this ambiguity likely arises from additional non-AMOC influences on the proxies or their varying sensitivity to different components of the AMOC. We suggest that enhanced freshwater fluxes from the Arctic and Nordic Seas, towards the end of the LIA, sourced from melting glaciers and thickened sea-ice that had developed earlier in the LIA, weakened Labrador Sea convection and the AMOC. The lack of a subsequent recovery may result from hysteresis or twentieth century melting of the Greenland ice sheet[6]. Our results highlight that recent decadal variability of Labrador Sea

convection and the AMOC has occurred during an atypical, weak background state. Future work should aim to constrain the role of internal climate variability versus early anthropogenic forcing in the AMOC weakening described here.

The AMOC is comprised of northward transport of warm surface and thermocline waters, and their deep southward return flow as dense waters that formed by cooling processes and sinking at high latitudes[2]. The stability of the AMOC in response to ongoing and projected climate change is uncertain. Monitoring of the AMOC by an array at 26°N, spanning the last decade, suggests a weakening of the AMOC, occurring ten times faster than expected from climate model projections[1]. However, it remains uncertain if this trend is part of a longer-term decline, natural multi-decadal variability, or a combination of both. Here, we develop past reconstructions of AMOC variability that can be directly compared to instrumental datasets and provide longer-term perspective.

The Labrador Sea is an important region for deep-water formation in the North Atlantic[5]. Moreover, modelling studies suggest that deep Labrador Sea density (dLSD) may be a useful predictor of AMOC change[3,4,7]. This is because density anomalies produced in the Labrador Sea - predominantly caused by varying deep convection - can propagate southwards rapidly (on the order of months) along the western margin via boundary waves, altering the cross-basin zonal density gradient, thus modifying geostrophic transport and therefore AMOC strength[2-4,7-9]. Building upon these studies, we show that dLSD anomalies are also associated with changes in the velocity of the deep western boundary current (DWBC) and the strength of the AMOC at 45°N in the high-resolution climate model HadGEM3-GC2 (see Methods and Fig. 1).

In addition to this link between the AMOC and dLSD and the DWBC, changes in AMOC also alter ocean heat transport. Modeling studies suggest that AMOC weakening affects the upper ocean heat content of the eastern subpolar gyre (SPG) with a lag time of ~10 years (ref. [10]), and a distinct AMOC fingerprint on subsurface temperature (Tsub, 400m water depth)[11] characterizes weak AMOC phases, with a dipole pattern of warming of the Gulf Stream extension region[12] and cooling of the subpolar Northeast Atlantic. We exploit the model-based covariance of decadal changes in AMOC with dLSD anomalies, SPG upper ocean heat content, and the Tsub fingerprint, to extend constraints on past AMOC variability (see Methods). Over the instrumental era (post ~1950), these indices suggest significant decadal variability in the AMOC, with coherent changes in dLSD, and lagged SPG upper ocean heat content and the Tsub AMOC fingerprint[3,5,8,10,11].

The model results in Figure 1 imply that we can use flow speed reconstructions of the DWBC to infer past changes in dLSD and AMOC. We analyzed the sortable silt (SS) mean grain size, a proxy for near-bottom current flow speed[13], in two marine sediment cores (48JPC and 56JPC; see Methods, Extended Data Fig. 1 and 2) located under the influence of southward flowing Labrador Sea Water (LSW) within the DWBC off Cape Hatteras (hereafter $DWBC_{LSW}$). The high accumulation rates (~0.5-1 cm/yr) and modern core-top enable direct comparison of the record from 56JPC to observational datasets (Fig. 2).

In agreement with the model-predicted relationship (i.e. Fig. 1), changes in inferred flow speed of the $DWBC_{LSW}$ show similar, in-phase, variability with observed deep Labrador Sea density[5]. Moreover, there is strong covariability of our $DWBC_{LSW}$ proxy with the lagged (12 year) SPG upper ocean heat content and Tsub index from observational analysis (Fig. 2a). Over the past ~100 years, the spatial correlation of upper ocean heat content anomalies associated with our $DWBC_{LSW}$ proxy closely resembles the Tsub AMOC fingerprint (Fig. 2b,c), supporting the concept that the $DWBC_{LSW}$ proxy and upper ocean temperature changes provide complementary, coherent, information on a common phenomenon, namely AMOC variability. Combined, these datasets imply that decadal variability has been a dominant feature of the past 130 years, with the most recent strengthening of LSW formation during the mid-1990s, and the subsequent decline, being particularly prominent features.

To gain insight prior to the instrumental era, we first extend our $DWBC_{LSW}$ flow speed reconstruction (Fig. 3e). The $DWBC_{LSW}$ proxy suggests that AMOC has been weaker during the last ~150 years than at any other time during the last 1600 years. The emergence of this weaker state (i.e.

smoothed record exceeds a noise threshold of 2σ pre-Industrial era variability), takes place at ~1880 CE in both cores. The overall transition occurs from ~1750 to ~1900 CE, late in the Little Ice Age (LIA, ~1350-1850 CE) and the early stages of the Industrial era (defined as ~1830 onwards[14]). Applying the flow speed calibration for sortable silt[13] suggests a decrease from 17 to 14.5 cm/s at 56JPC, and 14 to 12 cm/s at 48JPC, implying a decrease in $DWBC_{LSW}$ strength of ~15% (assuming constant $DWBC_{LSW}$ cross-sectional area). This decrease is equivalent to 3σ and 4σ of the pre-Industrial era variability in 48JPC and 56JPC, respectively.

Secondly, we compile quantitative proxy records of subsurface (~50-200m) ocean temperatures from key locations to extend the Tsub AMOC proxy (Fig. 3a-c; see Methods and Extended Data Fig. 3 & 4). The Tsub proxy reconstruction provides support for the proposed AMOC weakening. Opposing temperature anomalies recorded in the two regions after ~1830 CE, with warming of the Gulf Stream extension region and cooling of the subpolar Northeast Atlantic, together suggest a weaker Industrial-era AMOC. Further support for the AMOC weakening is suggested by the spatial pattern of Tsub change in the Northwest Atlantic during the onset of the Industrial era (Extended Data Fig. 5). In contrast to the prominent changes recorded in our proxy reconstructions at the end of the LIA, more subdued variability occurs during the earlier part of our records (400-1800 CE). This implies that the forcing and AMOC response was weaker, or it supports mechanisms in which the AMOC does not play a leading role in the (multi-)centennial climate variability of this period[15,16].

Labrador Sea deep convection is a major contributor to the AMOC, but susceptible to weakening[5]. Combined with its role in decadal variability over the last ~100 years (Fig. 2), and model analysis of mechanisms in operation today[8], it is likely that changes in Labrador Sea convection were involved in the weakening of AMOC at the end of the LIA. Additional correlative (not necessarily causative) support is revealed by paleoceanographic evidence from the Labrador Sea. Strong deep convection in the Labrador Sea is typically associated with cooling and freshening of the subsurface ocean[5]. Therefore, the reconstructed shift to warmer and saltier subsurface conditions in the northeast Labrador Sea[17] over the past ~150 years (Fig. 3d; equivalent to ~2σ of pre-Industrial era variability) is consistent with a shift to a state characterized by reduced deep convection, with only occasional episodes of sustained deep convection. Reconstructions of the other major deep-water contributors to the AMOC - the two Nordic Seas overflows - suggest that on centennial timescales they have varied in anti-phase and thus likely compensated for one another during the last 3000 years[18]. Hence, changes in Labrador Sea deep convection may have been the main cause of AMOC variability over this period.

While atmospheric circulation has played a dominant role in recent decadal variability of AMOC (and LSW)[2,8], there is no strong evidence that the AMOC decrease at the end of the LIA was similarly caused by a shift in atmospheric circulation[19]. Instead, we hypothesize that the AMOC weakening was caused by enhanced freshwater fluxes associated with the melting and export of ice and freshwater from the Arctic and Nordic Seas. During the LIA, circum-Arctic glaciers and multi-year Arctic and Nordic sea ice were at their most advanced state of the last few thousand years, and there were large ice-shelves in the Canadian Arctic and exceptionally thick multi-year sea-ice. Yet, by the early 20th century, many of these features had disappeared or were retreating[20-23].

Modelling studies suggest enhanced freshwater fluxes of ~10-100 mSv over a few decades can weaken Labrador Sea convection and AMOC[24], although models with strong hysteresis of Labrador Sea convection[25] suggest this may be as little as 5-10 mSv. Unfortunately, there is little data to constrain the Arctic and Nordic Seas freshwater fluxes associated with the end of the LIA. The earliest observational datasets suggest ~10 mSv from sea ice loss in the Arctic and Nordic Seas during 1895-1920[26,27], to which we must also add melting of previously expanded circum-Arctic glaciers and ice-shelves, and enhanced melting of the Greenland ice-sheet (GIS). Alternatively, we can estimate that a 1 m reduction in average Arctic sea-ice thickness during the termination of the LIA could yield a freshwater flux of 10 mSv for 50 years. While additional work is required to improve this incomplete estimate, there was likely sufficient freshwater stored in the Arctic and Nordic Seas during the LIA to impact Labrador Sea convection and AMOC.

The AMOC weakening recorded in our two marine reconstructions is broadly similar to that in a predominantly terrestrial-based AMOC proxy reconstruction[6] (Fig. 3c). Our Tsub AMOC proxy and the AMOC proxy of ref. 6 (Fig. 3c), both suggest a decline in AMOC through the 20th century, whereas our $DWBC_{LSW}$ AMOC proxy and the observational-based Tsub AMOC index (Fig. 2a and Extended Data Fig. 6) suggest no long-term AMOC decline during the 20th century. These differences may be attributed to several factors. Firstly, our sediment-core based Tsub proxy is subject to artificial smoothing, caused by combining numerous records with substantial (~10-100 year) individual age uncertainties, and compounded by bioturbation. Furthermore, the Tsub proxy sediment cores were retrieved in the late 1990s and early 2000s, therefore they cannot capture the strong Tsub index recovery from ~2000-2010 that reverses the earlier prolonged decline (see Extended Fig. 6). Alternatively, the earlier, more threshold-like change in the $DWBC_{LSW}$ AMOC proxy may be due to local shifts in the position of the DWBC, and/or non-linear dynamics of the DWBC response to AMOC change. However, based on the similarity of the $DWBC_{LSW}$ reconstructions from cores 56JPC and 48JPC, located at different water depths, and the strong correlation of $DWBC_{LSW}$ with Labrador Sea density and the Tsub AMOC index over the instrumental period, we suggest these factors are not substantial. Finally, the differences between the AMOC reconstructions may reflect their varying response timescales and sensitivities to the different components of the AMOC and the SPG[28,29].

Our study raises several issues regarding the modelling of AMOC in historical experiments. The inferred transition to a weakened AMOC occurred near the onset of the Industrial-era, several decades before the strongest global warming trend, and has remained weak up to the present day. This either suggests hysteresis of the AMOC in response to an early climate forcing – natural (solar, volcanic) or anthropogenic (greenhouse gases, aerosols, land-use change) - or alternatively, continued climate forcing, such as the melting of the GIS[6], has been sufficient to keep AMOC weak. Our reconstructions also differ from most climate model simulations, which show either negligible AMOC change or a later, more gradual reduction[30]. Many factors may be responsible for this model-data discrepancy: a misrepresentation of AMOC-related processes and possible hysteresis, including underestimation of AMOC sensitivity to climate (freshwater) forcing[29,31]; the underestimation or absence of important freshwater fluxes during the end of the LIA; and the lack of transient forced behaviour in the "constant forcing" pre-Industrial controls used to initialize historical forcings. Resolving these issues will be important for improving the accuracy of projected changes in AMOC.

In conclusion, our study reveals an anomalously weak AMOC over the last ~150 years. Because of its role in heat transport, it is often assumed that AMOC weakening cools the northern hemisphere. However, our study demonstrates that changes in AMOC are not always synchronous with temperature changes. That AMOC weakening occurred during the late LIA and onset of the Industrial era, rather than earlier in the LIA, may point to additional forcing factors at this time, such as an increase in the export of thickened Arctic and Nordic sea ice, or melting of circum-Arctic ice-shelves. The persistence of weak AMOC during the 20th century, when there was pronounced northern hemisphere and global warming, implies that other climate forcings, such as greenhouse gas warming, were dominant during this period. We therefore infer that AMOC has responded to recent centennial-scale climate change, rather than driven it. Regardless, the weak state of AMOC over the last ~150 years may have modified northward ocean heat transport, as well as atmospheric warming through altering ocean-atmosphere heat transfer[32,33], underscoring the need for continued investigation of the role of the AMOC in climate change. Determining the future behaviour of AMOC will depend in part on constraining its sensitivity and possible hysteresis to freshwater input, for which improved historical estimates of these fluxes during the AMOC weakening reported here will be especially useful.

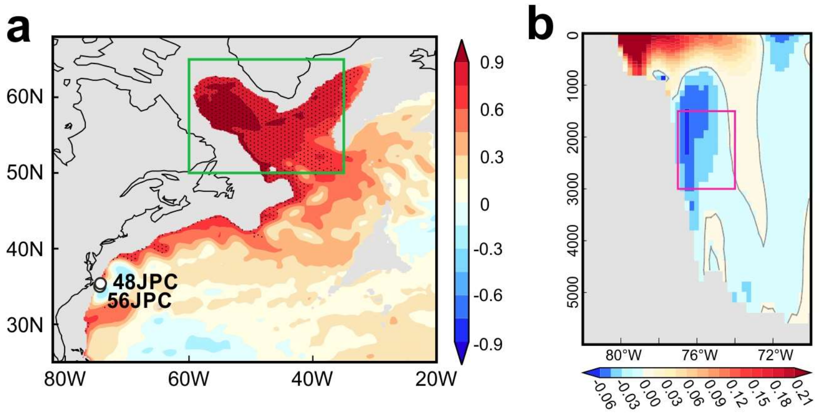

Fig. 1. Modelled link of DWBC velocity with deep Labrador Sea density and AMOC. a, Correlation of the vertically-averaged ocean density (1000-2500m) with dLSD; green box, 1000-2500m average) in HadGEM3-GC2 control run; cores sites for DWBC flow speed reconstruction shown. **b**, Climatology of the modelled meridional ocean velocity (ms^{-1}) 30-35ºN (see Methods and Extended Data Fig. 7&8), illustrating the modelled position of the DWBC. **c**, Cross-correlations between modelled averaged DWBC flow speed in pink box in **b** and indices of dLSD and AMOC at 45ºN (dashed line is without the Ekman component).

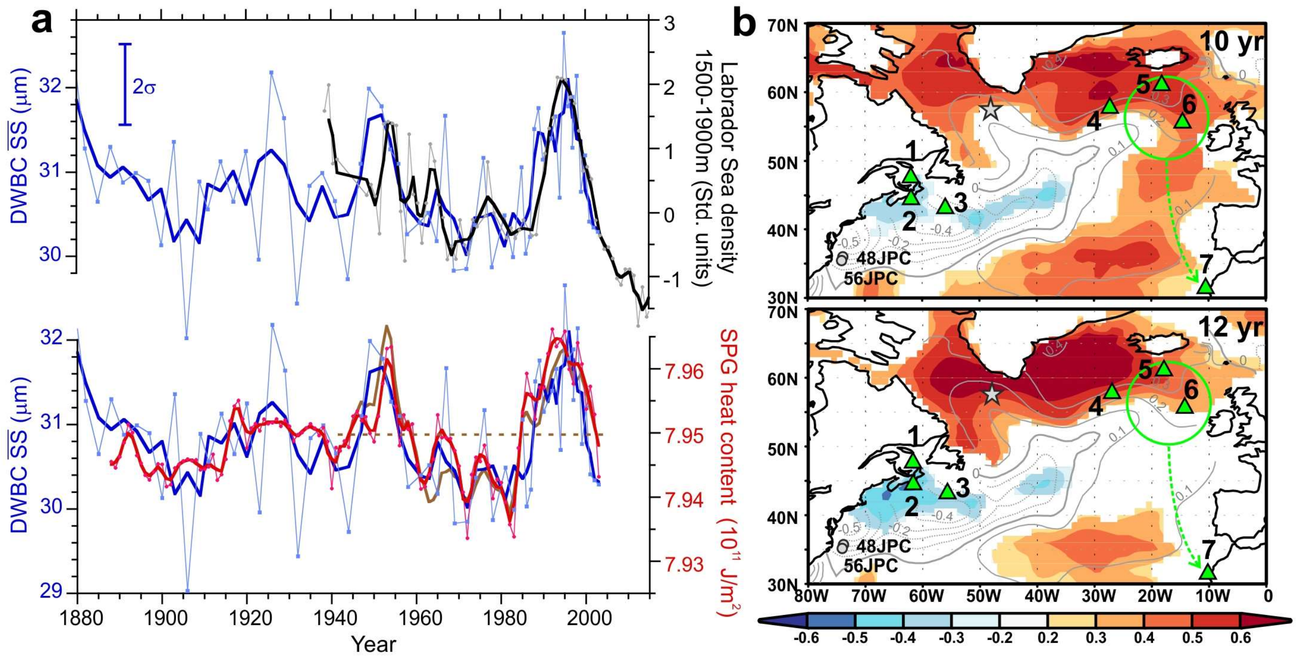

Fig. 2. Proxy validation and recent, multi-decadal variability. a, SS mean grain size (56JPC, blue) compared with: central Labrador Sea annual density[5] (black; r^2=0.56, n=54), comparable to model-based dLSD (Extended Data Fig. 9); and with 12-year lagged SPG upper ocean heat content (0-700m, 55-65ºN, 15-60ºW, EN4 dataset; red; r^2=0.58, n=116) and Tsub AMOC fingerprint[11] (brown; dashed line zero-line; r^2=0.76, n=55). Correlations (and 2σ SS error bar, n=30) are for 3-point means (bold). Low resolution 48JPC data not shown. **b**, 10- and 12-yr lagged spatial correlation of upper ocean heat content (0-700m) with reconstructed $DWBC_{LSW}$ flow speed (56JPC), heat content lags. Grey contours, spatial Tsub AMOC proxy[11]; green triangles, Tsub proxy sites; green circle, surface region controlling benthic temperatures at site 7. Grey circles, DWBC sites; grey star, core site ref. 17.

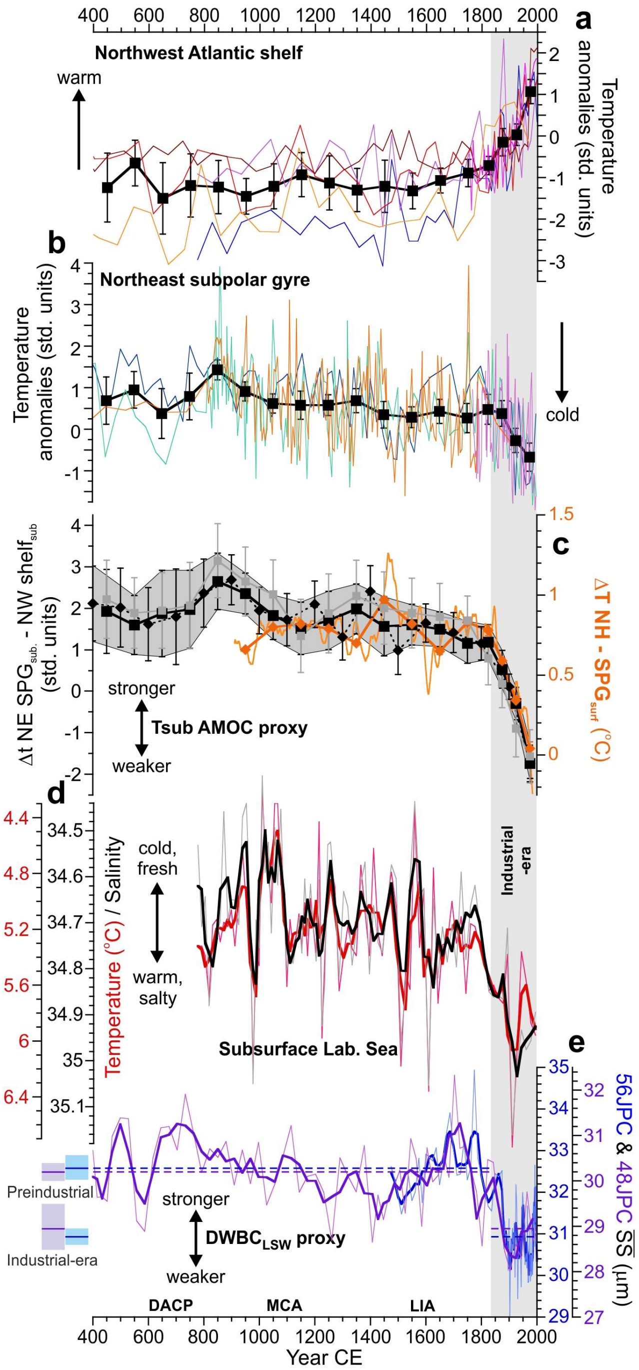

Fig. 3. Proxy reconstructions of AMOC changes over the last 1600 years. **a**,**b**, Subsurface Northwest Atlantic shelf (**a**) and Northeast Atlantic subpolar gyre (**b**) temperatures; sites in Fig. 2b; composite stacks, black. **c**, Tsub AMOC proxy (black, grey), various binning (see Extended Data Fig 4); orange, Rahmstorf AMOC proxy[6], 1ºC = ~2.3Sv, 21-yr smooth, thin line; thick line and symbols, binned as for Tsub AMOC proxy. **d**, *N. pachyderma* Mg/Ca-δ^{18}O subsurface (~100-200m) temperature and salinity for northeast Labrador Sea[17]. **e**, SS mean grain size (56JPC, blue; 48JPC, purple; bold, 3-point means); dashed lines, Industrial/Preindustrial-era averages. Error bars/shading, ±2SE. DACP (Dark Ages Cold Period, ~400-800 CE), MCA (Medieval Climate Anomaly, ~900-1250 CE).

References

1. Srokosz, M. A. & Bryden, H. L. Observing the Atlantic Meridional Overturning Circulation yields a decade of inevitable surprises. Science 348, doi:10.1126/science.1255575 (2015).
2. Buckley, M. W. & Marshall, J. Observations, inferences, and mechanisms of the Atlantic Meridional Overturning Circulation: A review. Reviews of Geophysics 54, 5-63, doi:10.1002/2015RG000493 (2016).
3. Jackson, L. C., Peterson, K. A., Roberts, C. D. & Wood, R. A. Recent slowing of Atlantic overturning circulation as a recovery from earlier strengthening. Nature Geosci 9, 518-522, doi:10.1038/ngeo2715 (2016).
4. Robson, J., Hodson, D., Hawkins, E. & Sutton, R. Atlantic overturning in decline? Nature Geosci 7, 2-3, doi:10.1038/ngeo2050 (2014).
5. Yashayaev, I. Hydrographic changes in the Labrador Sea, 1960–2005. Progress in Oceanography 73, 242-276, doi: 10.1016/j.pocean.2007.04.015 (2007).
6. Rahmstorf, S. et al. Exceptional twentieth-century slowdown in Atlantic Ocean overturning circulation. Nature Clim. Change 5, 475-480, doi:10.1038/nclimate2554 (2015).
7. Hodson, D. L. R. & Sutton, R. T. The impact of resolution on the adjustment and decadal variability of the Atlantic meridional overturning circulation in a coupled climate model. Climate Dynamics 39, 3057-3073, doi:10.1007/s00382-012-1309-0 (2012).
8. Ortega, P., Robson, J., Sutton, R. T. & Andrews, M. B. Mechanisms of decadal variability in the Labrador Sea and the wider North Atlantic in a high-resolution climate model. Climate Dynamics, doi:10.1007/s00382-016-3467-y (2016).
9. Roberts, C. D., Garry, F. K. & Jackson, L. C. A Multimodel Study of Sea Surface Temperature and Subsurface Density Fingerprints of the Atlantic Meridional Overturning Circulation. Journal of Climate 26, 9155-9174, doi:10.1175/jcli-d-12-00762.1 (2013).
10. Robson, J., Ortega, P. & Sutton, R. A reversal of climatic trends in the North Atlantic since 2005. Nature Geosci 9, 513-517, doi:10.1038/ngeo2727 (2016).
11. Zhang, R. Coherent surface-subsurface fingerprint of the Atlantic meridional overturning circulation. Geophysical Research Letters 35, doi:10.1029/2008GL035463 (2008).
12. Saba, V. S. et al. Enhanced warming of the Northwest Atlantic Ocean under climate change. Journal of Geophysical Research: Oceans 121, 118-132, doi:10.1002/2015JC011346 (2016).
13. McCave, I. N., Thornalley, D. J. R. & Hall, I. R. Relation of sortable silt grain-size to deep-sea current speeds: Calibration of the 'Mud Current Meter'. Deep Sea Research Part I: Oceanographic Research Papers, doi:10.1016/j.dsr.2017.07.003 (2017).
14. Abram, N. J. et al. Early onset of industrial-era warming across the oceans and continents. Nature 536, 411-418, doi:10.1038/nature19082 (2016).

15. Moreno-Chamarro, E., Zanchettin, D., Lohmann, K. & Jungclaus, J. H. An abrupt weakening of the subpolar gyre as trigger of Little Ice Age-type episodes. Climate Dynamics 48, 727-744, doi:10.1007/s00382-016-3106-7 (2017).

16. Miller, G. H. et al. Abrupt onset of the Little Ice Age triggered by volcanism and sustained by sea-ice/ocean feedbacks. Geophysical Research Letters 39, doi:10.1029/2011gl050168 (2012).

17. Moffa-Sánchez, P., Hall, I. R., Barker, S., Thornalley, D. J. R. & Yashayaev, I. Surface changes in the eastern Labrador Sea around the onset of the Little Ice Age. Paleoceanography 29, 160-175, doi:10.1002/2013PA002523 (2014).

18. Moffa-Sanchez, P., Hall, I. R., Thornalley, D. J. R., Barker, S. & Stewart, C. Changes in the strength of the Nordic Seas Overflows over the past 3000 years. Quaternary Science Reviews 123, 134-143, doi: 10.1016/j.quascirev.2015.06.007 (2015).

19. Ortega, P. et al. A model-tested North Atlantic Oscillation reconstruction for the past millennium. Nature 523, 71-74, doi:10.1038/nature14518 (2015).

20. Bradley, R. S. & England, J. H. The Younger Dryas and the Sea of ancient ice. Quaternary Research 70, 1-10 (2008).

21. Funder, S. et al. A 10,000-Year Record of Arctic Ocean Sea-Ice Variability—View from the Beach. Science 333, 747-750, doi:10.1126/science.1202760 (2011).

22. Vincent, W. F., Gibson, J. A. E. & Jeffries, M. O. Ice-shelf collapse, climate change, and habitat loss in the Canadian high Arctic. Polar Record 37, 133-142, doi:10.1017/S0032247400026954 (2001).

23. Cabedo-Sanz, P., Belt, S. T., Jennings, A. E., Andrews, J. T. & Geirsdóttir, Á. Variability in drift ice export from the Arctic Ocean to the North Icelandic Shelf over the last 8000 years: A multi-proxy evaluation. Quaternary Science Reviews 146, 99-115, doi:http://dx.doi.org/10.1016/j.quascirev.2016.06.012 (2016).

24. Yang, Q. et al. Recent increases in Arctic freshwater flux affects Labrador Sea convection and Atlantic overturning circulation. 7, 10525, doi:10.1038/ncomms10525 (2016).

25. Schulz, M., Prange, M. & Klocker, A. Low-frequency oscillations of the Atlantic Ocean meridional overturning circulation in a coupled climate model. Climate of the Past 3, 97-107 (2007).

26. Polyakov, I. V. et al. Arctic Ocean Freshwater Changes over the Past 100 Years and Their Causes. Journal of Climate 21, 364-384, doi:10.1175/2007jcli1748.1 (2008).

27. Vinje, T. Anomalies and Trends of Sea-Ice Extent and Atmospheric Circulation in the Nordic Seas during the Period 1864–1998. Journal of Climate 14, 255-267, doi:10.1175/1520-0442(2001)014<0255:aatosi>2.0.co;2 (2001).

28. Drijfhout, S., Oldenborgh, G. J. v. & Cimatoribus, A. Is a Decline of AMOC Causing the Warming Hole above the North Atlantic in Observed and Modeled Warming Patterns? Journal of Climate 25, 8373-8379, doi:10.1175/jcli-d-12-00490.1 (2012).

29. Sgubin, G., Swingedouw, D., Drijfhout, S., Mary, Y. & Bennabi, A. Abrupt cooling over the North Atlantic in modern climate models. 8, doi:10.1038/ncomms14375 (2017).

30. Weaver, A. J. et al. Stability of the Atlantic meridional overturning circulation: A model intercomparison. Geophysical Research Letters 39, doi:10.1029/2012gl053763 (2012).

31. Liu, W., Xie, S.-P., Liu, Z. & Zhu, J. Overlooked possibility of a collapsed Atlantic Meridional Overturning Circulation in warming climate. Science Advances 3, doi:10.1126/sciadv.1601666 (2017).

32. Drijfhout, S. Competition between global warming and an abrupt collapse of the AMOC in Earth's energy imbalance. Scientific Reports 5, 14877, doi:10.1038/srep14877 (2015).

33. Kostov, Y., Armour, K. C. & Marshall, J. Impact of the Atlantic meridional overturning circulation on ocean heat storage and transient climate change. *Geophysical Research Letters* **41**, 2108-2116, doi:10.1002/2013GL058998 (2014).

Acknowledgements

We thank Ellen Roosen for help with core sampling, Henry Abrams, Sean O'Keefe, Kathryn Pietro, Lindsey Owen and Francesco Pallottino for assistance in processing sediment samples; Kitty Green for faunal counts in 10MC; Martin Andrews at the UK Met Office for providing the model data; and Stefan Rahmstorf for useful suggestions. Funding was provided by NSF grant OCE-1304291 to DO, DT, LK; NERC Project DYNAMOC (NE/M005127/1) to PO and JR; NERC LTSM ACSIS to JR; by the Leverhulme Trust and ATLAS to DT. This project has received funding from the European Union's Horizon 2020 research and innovation programme under grant agreement No 678760 (ATLAS). This output reflects only the authors' views and the European Union cannot be held responsible for any use that may be made of the information contained therein.

Author contributions

Conceived by DT; NSF project proposal written and managed by DO and DT; cores 56JPC and 48JPC collected by LK; SS analysis and interpretation by DT, with contributions from PS and RD; modelling work by PO and JR; SCP analysis by NR; Monte-Carlo modeling by PS; first draft written by DT; all authors contributed to discussion and final version of the manuscript.

Author Information

The authors declare no competing financial interests.

Correspondence and requests for materials should be addressed to d.thornalley@cantab.net

METHODS

Climate model investigation of AMOC and DWBC changes

The climate model used in this study was the UK Met Office's Third Hadley Centre Global Environmental Model – Global Coupled Configuration two (HadGEM3–GC2). The ocean model for HadGEM3-GC2 is the Global Ocean version 5.0, which is based on the version 3.4 of the Nucleus for European Models of the Ocean model (NEMO)[34]. The ocean model has 75 vertical levels, and is run at a nominal ¼° resolution using the NEMO tri-polar grid. The atmospheric component is the Global Atmosphere version 6.0 of the UK Met Office Unified Model, and is run at N216 resolution (~60km in mid-latitudes), with 85 vertical levels. More information on the model can be found in Williams et al[35]. The experiment analyzed here was a 310-year control simulation of HadGEM3-GC2, i.e. it includes no changes in external forcings. This experiment was previously run and analyzed in Ortega et al[8], where details of the specific model experiment are included. This coupled simulation has a relatively high spatial resolution for a more accurate representation of the boundary currents, and is sufficiently long to resolve a large number of decadal oscillations. All model data has been linearly detrended to remove any potential drift, and smoothed with a 10-year running mean in order to focus on the decadal and multi-decadal variability.

We use the model-based relationships to support the interpretation of the proxy-based AMOC reconstructions, which cannot be validated with the limited observations available. The AMOC at 45°N is chosen as this is the latitude with the largest correlations with both the deep Labrador Sea Density (dLSD) and deep western boundary current (DWBC) velocity index in the model. Note that AMOC indices defined at other latitudes (e.g. 35°N, 40°N) produce weaker, but still significant correlations with both dLSD and the DWBC. The simulated DWBC velocity index is the average of 30-35°N as at 35°N (the latitude where the sediment cores were taken) the DWBC is found offshore, which we believe is associated with the model's Gulf Stream separating further north than in the observations (Extended Data Fig. 7). It should be noted, however, that changes in the position of the observed Gulf Stream do not appear to directly control the reconstructed flow speed changes in the $DWBC_{LSW}$ (see Extended Data Fig. 10).

We have also assessed the robustness of the model-based relationships to the smoothing. For example we reproduced the cross-correlation analysis in Fig. 1c using undetrended and/or unsmoothed data instead. In all cases, the lead-lags relationships are similar, with larger correlations emerging when the decadal smoothing is applied. Furthermore, we also tested the sensitivity of the model-based relationships to the specific model used. In particular, we repeated the analysis of Fig. 1 in the 340 year control experiment using the HiGEM climate model[36]. HiGEM has a similar horizontal ocean resolution (1/3°), but is based on a different ocean model. Encouragingly, Extended Data Fig. 8 shows that the results are consistent across the two models, in particular the link between dLSD and the DWBC, and between the DWBC and the AMOC at 45°N. However, there are some caveats. For example, both models' Gulfstream separate too far north, which led us to define the DWBC flow indices slightly south of the core sites. HiGEM also has a deeper DWBC than HadGEM3-GC2. Therefore, the DWBC index was computed at different levels in both models in order to represent the link between dLSD and the DWBCs. However, despite these differences, both models support the general interpretation that the DWBC in the vicinity of Cape Hatteras is strongly connected with changes in the dLSD and the AMOC.

The interpretation of the model results is consistent with previously published model studies (both low and high resolution) that have revealed a coupling between the AMOC and/or Labrador Sea density, and the DWBC[3,7,11,37]. These modelled relationships support a causal link for the correlations between the instrumental records of Labrador Sea density and the reconstructed DWBC velocity, presented in Fig 2. Furthermore, recent instrumental data of the DWBC at 39°N spanning 2004-2014 reveal that a reduction in the velocity of classical LSW within the DWBC is also accompanied by a decrease in its density[38], as hypothesized here. The observed decrease in the velocity and density of classical LSW within the DWBC between 2004 and 2014 is also consistent with the decrease in the density of the deep Labrador Sea over this period (Fig. 2a and Extended Data Fig. 9), although a longer observational DWBC time-series is needed to gain confidence in this relationship.

Age models

New and updated age models for the cores are presented in Extended Figures 1 & 2, and are based on ^{14}C, ^{210}Pb and spheroidal carbonaceous particle (SCP) concentration profiles[39].

Sortable silt data

Two marine sediment cores were used for DWBC flow speed reconstruction: KNR-178-56JPC (~35°28'N, 74°43'W, 1718 m water depth) and KNR-178-48JPC (35°46'N, 74°27'W, 2009 m water depth). Sediments were processed using established methods[40] taking 1cm wide samples, every 1cm for the top 63cm and then every 4cm down to 200cm in 56JPC, and every 1cm down to 71cm in 48JPC. Samples were analyzed at Cardiff University on a Beckman Coulter Multisizer 4 using the Enhanced Performance Multisizer 4 beaker and stirrer setting 30 to ensure full sediment suspension. Two or three separate aliquots were analyzed for each sample, sizing 70,000 particles per aliquot. Analytical precision was ~1% (±0.3μm), whilst full procedural error (based on replicates of ~25% of samples, starting from newly sampled bulk sediment) was ±0.8μm.

Temperature data and constructing the Tsub index

Numerous studies have suggested AMOC variability is associated with a distinct surface or subsurface (400m) temperature fingerprint in the North Atlantic[6,11,28,41]. However, the lack of long-term observations of AMOC prevents accurate diagnosis of the precise AMOC temperature fingerprint, and models display a range of different AMOC temperature fingerprints[9,42]. In this study we focus on the Tsub AMOC fingerprint, proposed by Zhang[11] on the basis of covariance between modelled AMOC, the spatial pattern of the leading mode of subsurface (400m) temperature variability, and sea-surface height changes. These model-based relationships were supported by similar relationships (spatial and temporal) observed in recent instrumental data of subsurface temperature and sea surface height. The agreement between our $DWBC_{LSW}$ AMOC reconstruction, observed Labrador Sea density changes, and the Tsub AMOC fingerprint, provides support for our approach and suggests the Tsub AMOC fingerprint is capturing an important component of deep AMOC variability. Differences between the various proposed AMOC temperature fingerprints likely reflects their sensitivity to different aspects of AMOC and heat transport in the North Atlantic e.g. AMOC versus SPG circulation[28]; the temperature response to each of these components may be resolved if more comprehensive spatial networks of past North Atlantic temperature variability are generated[43].

Records used in the OCEAN 2K synthesis[44] from the Northwest Atlantic slope and the subpolar Northeast Atlantic were selected and supplemented with additional records that also record past temperature variability in the subsurface ocean of the chosen region. Cores that did not have a modern core top age (1950 CE or younger) or resolution of better than 100 years were not included. Foraminiferal-based temperature proxies were selected because they record subsurface temperatures (typically 50-200m), upon which the Tsub proxy is based. We avoid other temperature proxies (e.g.

alkenones, coccolithores, diatoms) that are typically more sensitive to sea surface temperature, rather than Tsub, and which also use the fine fraction that at the drift sites required for the necessary age resolution contains significant allochthonous material, compromising the fidelity of *in situ* temperature reconstruction[45,46].

All Tsub records were normalized to the interval 1750-2000 CE (the length of the shortest records). The Tsub proxy reconstruction was calculated as the difference between the stacked temperature records of the Northwest and Northeast Atlantic. Our results are insensitive to the precise binning or stacking method, as shown in Extended Data Fig. 4. The sedimentation rates of the cores used, combined with the effects of bioturbation mean we cannot resolve signals on timescales shorter than ~20-50 years. Age model uncertainty is estimated to be up to ~30 years for the last ~150 years where cores have ^{210}Pb dating, and ~100 years for 400-1800 CE where ^{14}C dating is relied upon. Therefore, the optimal bin intervals chosen were 50 years for 1800-2000 CE, and 100 years for 400-1800 CE. Results for only using 50 year and 100 year bins, as well as 30 year bins for the top 200 years, are shown in Extended Data Fig. 4.

Data Availability

The proxy data that support these findings are provided with the paper as Source Data for Fig. 2, 3, Extended Data Fig 1, 2, 4, 5, 6, 9, and at NGDC Paleoclimatology (https://www.ncdc.noaa.gov/data-access/paleoclimatology-data/datasets). Model data can be made available from Jon Robson (j.i.robson@reading.ac.uk) upon reasonable request.

References

34. Megann, A. et al. GO5.0: the joint NERC–Met Office NEMO global ocean model for use in coupled and forced applications. Geosci. Model Dev. 7, 1069-1092, doi:10.5194/gmd-7-1069-2014 (2014).

35. Williams, K. D. et al. The Met Office Global Coupled model 2.0 (GC2) configuration. Geosci. Model Dev. 8, 1509-1524, doi:10.5194/gmd-8-1509-2015 (2015).

36. Shaffrey, L. C. et al. U.K. HiGEM: The New U.K. High-Resolution Global Environment Model—Model Description and Basic Evaluation. Journal of Climate 22, 1861-1896, doi:10.1175/2008jcli2508.1 (2009).

37. Bakker, P., Govin, A., Thornalley, D. J. R., Roche, D. M. & Renssen, H. The evolution of deep-ocean flow speeds and δ13C under large changes in the Atlantic overturning circulation: Toward a more direct model-data comparison. Paleoceanography 30, 95-117, doi:10.1002/2015PA002776 (2015).

38. Toole, J. M., Andres, M., Le Bras, I. A., Joyce, T. M. & McCartney, M. S. Moored observations of the Deep Western Boundary Current in the NWAtlantic: 2004–2014. Journal of Geophysical Research: Oceans 122, 7488-7505, doi:10.1002/2017JC012984 (2017).

39. Rose, N. L. Spheroidal Carbonaceous Fly Ash Particles Provide a Globally Synchronous Stratigraphic Marker for the Anthropocene. Environmental Science & Technology 49, 4155-4162, doi:10.1021/acs.est.5b00543 (2015).

40. McCave, I. N., Manighetti, B., Robinson, S.G. Sortable silt and fine sediment size/composition slicing: Parameters for palaeocurrent speed and palaeoceanography. Paleoceanography 10, 593-610 (1995).

41. Dima, M. & Lohmann, G. Evidence for Two Distinct Modes of Large-Scale Ocean Circulation Changes over the Last Century. Journal of Climate 23, 5-16, doi:10.1175/2009jcli2867.1 (2010).

42. Muir, L. C. & Fedorov, A. V. How the AMOC affects ocean temperatures on decadal to centennial timescales: the North Atlantic versus an interhemispheric seesaw. Climate Dynamics 45, 151-160, doi:10.1007/s00382-014-2443-7 (2015).

43. Ortega, P., Robson, J., Moffa-Sanchez, P., Thornalley, D. J. R. & Swingedouw, D. A last millennium perspective on North Atlantic variability: exploiting synergies between models and proxy data. *CLIVAR exchanges* **72**, 61-67, doi:10.22498/pages.25.1 (2017).

44. McGregor, H. V. et al. Robust global ocean cooling trend for the pre-industrial Common Era. Nature Geosci 8, 671-677, doi:10.1038/ngeo2510 (2015).

45. McCave, I. N. A Poisoned Chalice? Science 298, 1186-1187, doi:10.1126/science.1076960 (2002).

46. Filippova, A., Kienast, M., Frank, M. & Schneider, R. R. Alkenone paleothermometry in the North Atlantic: A review and synthesis of surface sediment data and calibrations. Geochemistry, Geophysics, Geosystems 17, 1370-1382, doi:10.1002/2015GC006106 (2016).

47. Marchitto, T. & deMenocal, P. Late Holocene variability of upper North Atlantic Deep Water temperature and salinity. Geochemistry Geophysics Geosystems 4, 1100, doi:1110.1029/2003GC000598 (2003).

48. Keigwin, L. D., Sachs, J. P. & Rosenthal, Y. A 1600-year history of the Labrador Current off Nova Scotia. Climate Dynamics 21, 53-62, doi:10.1007/s00382-003-0316-6 (2003).

49. Keigwin, L. D. & Pickart, R. S. Slope Water Current over the Laurentian Fan on Interannual to Millennial Time Scales. Science 286, 520-523, doi:10.1126/science.286.5439.520 (1999).

50. Genovesi, L. et al. Recent changes in bottom water oxygenation and temperature in the Gulf of St. Lawrence: Micropaleontological and geochemical evidence. Limnology and Oceanography 56, 1319-1329, doi:10.4319/lo.2011.56.4.1319 (2011).

51. Hall, I. R., Boessenkool, K. P., Barker, S., McCave, I. N. & Elderfield, H. Surface and deep ocean coupling in the subpolar North Atlantic during the last 230 years. Paleoceanography 25, n/a-n/a, doi:10.1029/2009PA001886 (2010).

52. Moffa-Sanchez, P., Born, A., Hall, I. R., Thornalley, D. J. R. & Barker, S. Solar forcing of North Atlantic surface temperature and salinity over the past millennium. Nature Geosci 7, 275-278, doi:10.1038/ngeo2094 (2014).

53. Thornalley, D. J. R., Elderfield, H. & McCave, I. N. Holocene oscillations in temperature and salinity of the surface subpolar North Atlantic. Nature 457, 711-714, doi:10.1038/nature07717 (2009).

54. Richter, T. O., Peeters, F. J. C. & van Weering, T. C. E. Late Holocene (0-2.4 ka BP) surface water temperature and salinity variability, Feni Drift, NE Atlantic Ocean. Quaternary Science Reviews 28, 1941-1955, doi:10.1016/j.quascirev.2009.04.008 (2009).

55. Morley, A. et al. Solar modulation of North Atlantic central Water formation at multidecadal timescales during the late Holocene. Earth and Planetary Science Letters 308, 161-171, doi:10.1016/j.epsl.2011.05.043 (2011).

56. Morley, A., Rosenthal, Y. & deMenocal, P. Ocean-atmosphere climate shift during the mid-to-late Holocene transition. Earth and Planetary Science Letters 388, 18-26, doi: 10.1016/j.epsl.2013.11.039 (2014).

57. Sicre, M.-A. et al. A 4500-year reconstruction of sea surface temperature variability at decadal time-scales off North Iceland. Quaternary Science Reviews 27, 2041-2047, doi:10.1016/j.quascirev.2008.08.009 (2008).

58. Joyce, T. M. & Zhang, R. On the Path of the Gulf Stream and the Atlantic Meridional Overturning Circulation. Journal of Climate 23, 3146-3154, doi:10.1175/2010jcli3310.1 (2010).

59. Suman, D. O. & Bacon, M. P. Variations in Holocene sedimentation in the North American Basin determined from 230Th measurements. Deep Sea Research Part A. Oceanographic Research Papers 36, 869-878, doi: 10.1016/0198-0149(89)90033-2 (1989).

560. Adkins, J. F., Boyle, E. A., Keigwin, L. & Cortijo, E. Variability of the North Atlantic thermohaline circulation during the last interglacial period. Nature 390, 154-156, doi:10.1038/36540 (1997).

61. Hodson, D. L. R., Robson, J. I. & Sutton, R. T. An Anatomy of the Cooling of the North Atlantic Ocean in the 1960s and 1970s. Journal of Climate 27, 8229-8243, doi:10.1175/jcli-d-14-00301.1 (2014).

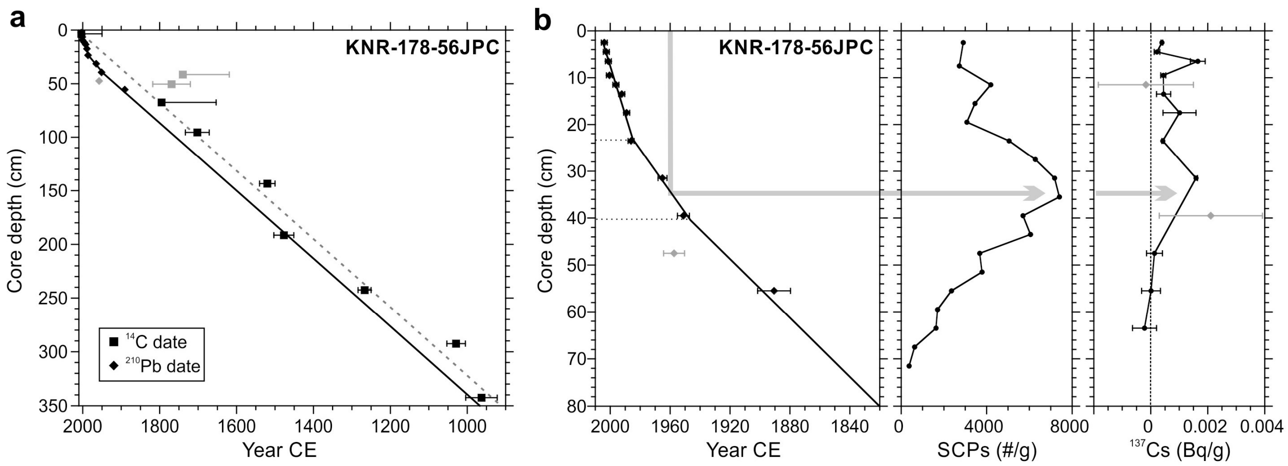

Extended Data Figure 1. Age model for core KNR-178-56JPC. a, ^{14}C and ^{210}Pb dating. ^{14}C ages (with 1σ ranges; grey, rejected dates) on planktonic foraminifera yielded a modern core top age and indicate an average sedimentation rate over the last 1000 years of 320cm/kyr (dashed line). The presence throughout the core of abundant lithogenic grains in the >150μm fraction, alongside the coarse sortable silt mean grain size values, suggest some reworking of foraminifera is likely, resulting in average ^{14}C ages that may be slightly (~50 years) older than their final depositional age, consistent with the ^{210}Pb dates not splicing smoothly into the ^{14}C ages (^{14}C ages appear slightly too old). The final age model was therefore based on the ^{210}Pb ages for the last century, and was then simply extrapolated back in time using the linear sedimentation rate of 320cm/kyr. Given that none of our findings are dependent on close age control in the older section of this core (i.e. pre 1880 CE), this uncertainty (converted ^{14}C ages are ~50 years older than the extrapolated linear age model) does not affect the conclusions of our study. **b**, The age model for the top 80cm of 56JPC is based on ^{210}Pb dating of bulk sediment assuming the constant initial concentration (CIC) method (rejecting the date at 47cm – likely burrow). A simple two-segment linear fit to the ^{210}Pb dates was adopted (rather than point-to-point interpolation or a spline) because sedimentological evidence - an abrupt increase in the % coarse fraction at 23cm depth, not observed elsewhere in the core, is indicative of a step change in the sedimentation rate. Further support for the age model of 56JPC over the last century is derived from the down-core abundance profile of spheroidal carbonaceous particles (SCPs, derived from high temperature fossil fuel combustion, counted using the methods described in ref. [39]) which ramped up from the mid-late 1800s and peaked in the 1950s-70s (40 to 25cm) before declining over recent decades, consistent with the ^{210}Pb based age model. The occurrence of ^{137}Cs in the top ~40cm of the core is also consistent with the ^{210}Pb based age of ~1950 at 40cm. Age uncertainty (1σ) for the last 60 years of the core is estimated at ±2-3 years. Note, sediment core top is at 3cm depth in core-liner.

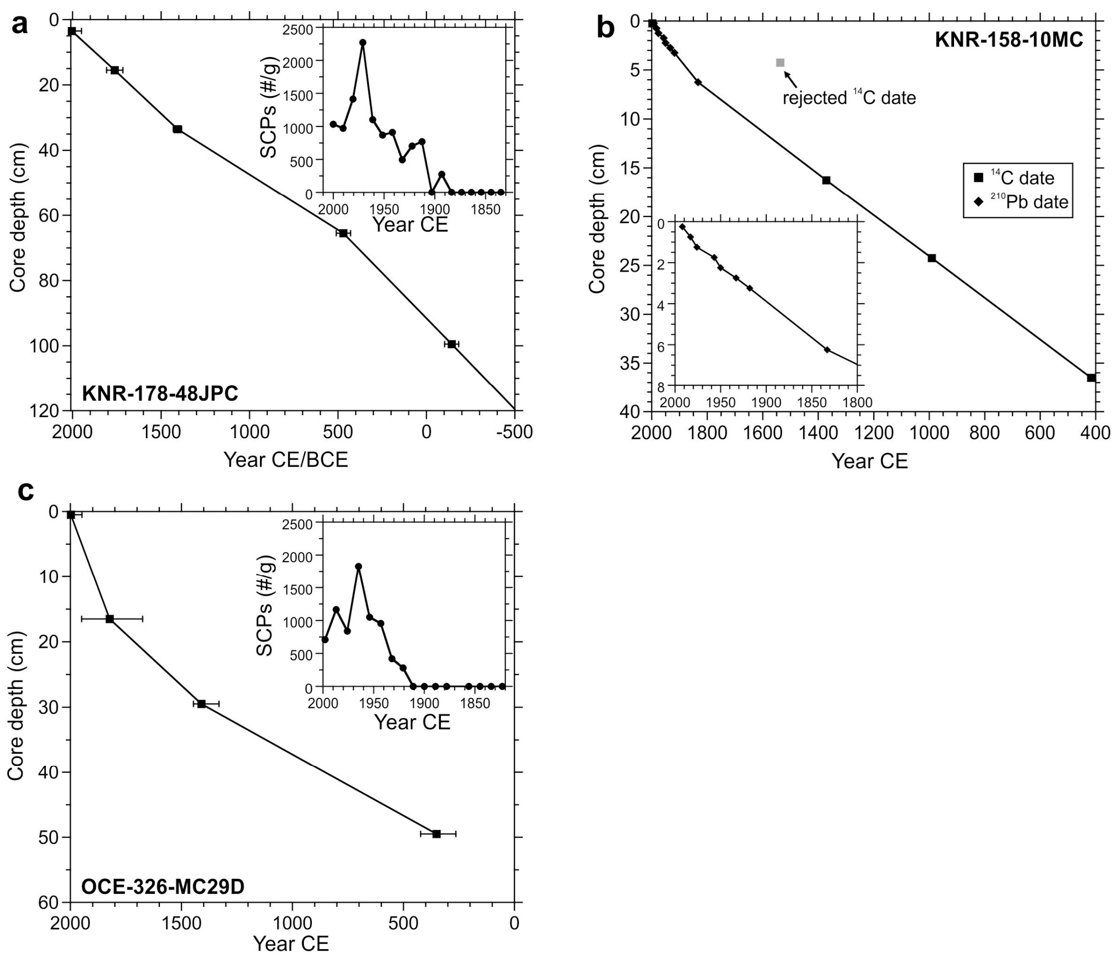

Extended Data Figure 2. Age models for additional cores. a, ^{14}C age model based on linear interpolation of ^{14}C dated planktic foraminifera (with 1σ ranges) in sediment core KNR-178-48JPC (used for the $DWBC_{LSW}$ SS reconstruction); yielding a modern core top age and average sedimentation rate of ~50cm/kyr. Note, core top is at 3cm depth in core-liner. Insert shows the SCP profile for 48JPC based on the ^{14}C age model, confirming the modern age of the top sediments, with SCPs showing the expected profile: increasing from the late 1800s onwards, peaking ~1950-1970 and then declining afterwards. **b**, Updated age model for KNR-158-10MC (after ref. [47]; used in Extended Data Fig. 1, examining regional near surface temperature trends in the NW Atlantic during the Industrial era) using new ^{210}Pb dating (CIC method) for the top 7cm and rejecting the anomalously old ^{14}C age at 4cm depth. A single detectable occurrence of ^{137}Cs at 2-2.5cm (equivalent to 1957 on the ^{210}Pb based age model) can be linked to the bomb peak at 1963, supporting the age model. Also note, SCPs were found in the top 5cm of this core, confirming the Industrial era age for the top 5cm, however the low concentrations prevent meaningful interpretation of the down-core trends and are not shown. **c,** Age model for core OCE-326-MC29B (used for Tsub reconstruction of the NW Atlantic shelf). ^{14}C ages of planktic foraminifera (with 1σ ranges) from ref. [48] . Support for this age model is provided by the SCP concentrations (this study) which show the expected down-core profile[39] when plotted using the ^{14}C ages. ^{210}Pb dating[48] also suggests a sedimentation rate of ~120cm/kyr for uppermost sediments, consistent with the ^{14}C ages and SCP profile.

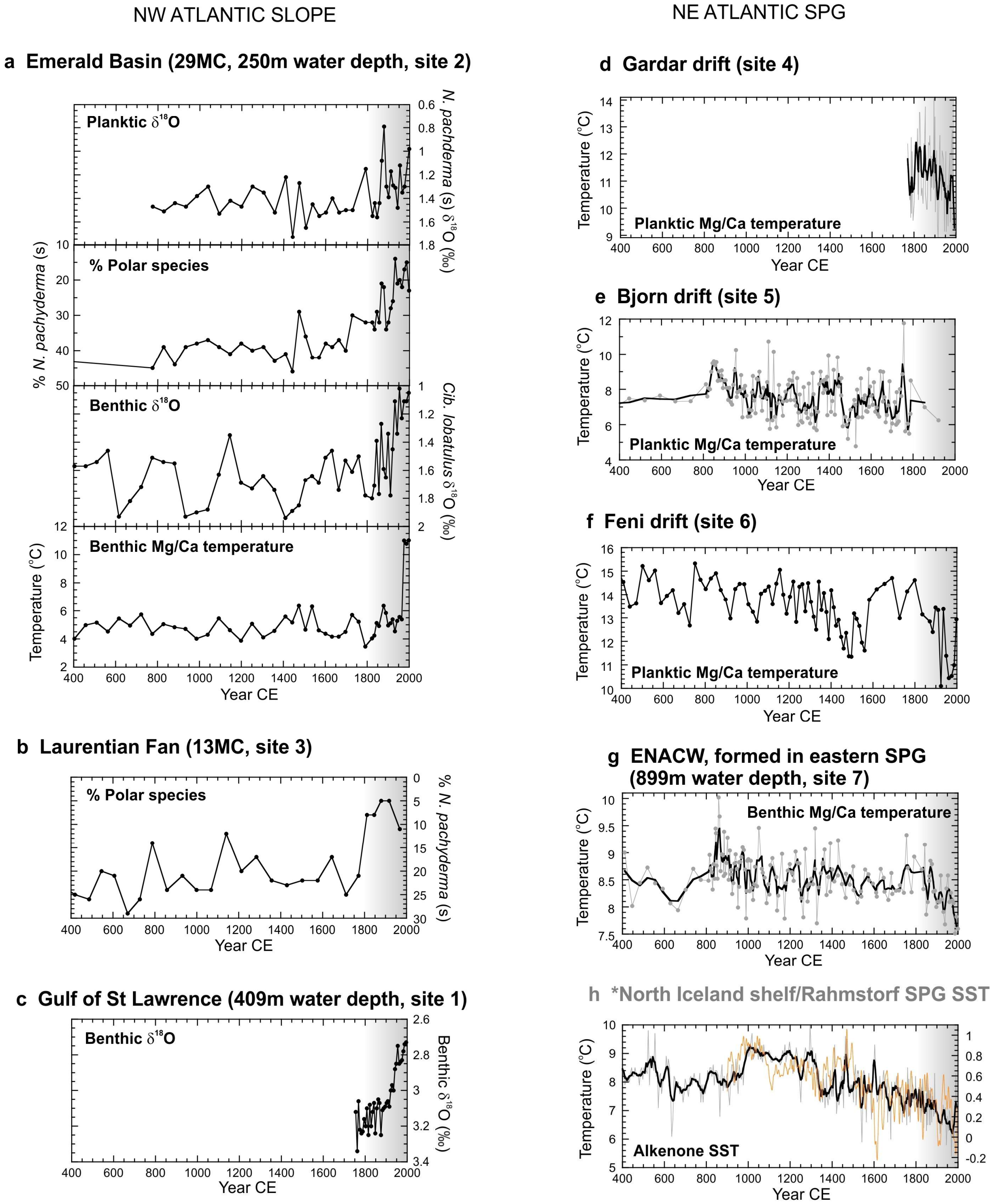

Extended Data Figure 3. Raw data for construction of Tsub AMOC proxy shown in Fig. 3. Locations are shown in Fig. 2b. **a-c,** Temperature proxy records from refs[48-50] used for the Northwest Atlantic stack, where model studies[11,12] indicate AMOC weakening results in warming of the surface and subsurface waters. **d-g,** records used to reconstruct Northeast Atlantic subpolar gyre subsurface temperatures: **d,** Gardar drift[51], **e,** combined South Iceland data[52,53], **f,** Feni drift[54], **g,** Eastern North Atlantic Central Water (ENACW) largely composed of waters formed in the eastern SPG[55,56], **h,** The high resolution alkenone SST record from the North Iceland shelf[57] was not included because it is not located within the open North Atlantic subpolar gyre, although it does also show the lowest temperature of the last 1600 years occurred during the most recent century, similar to the other Northeast Atlantic records. Also shown for reference is the Rahmstorf central subpolar gyre SST reconstruction (largely based on terrestrial proxies)[6].

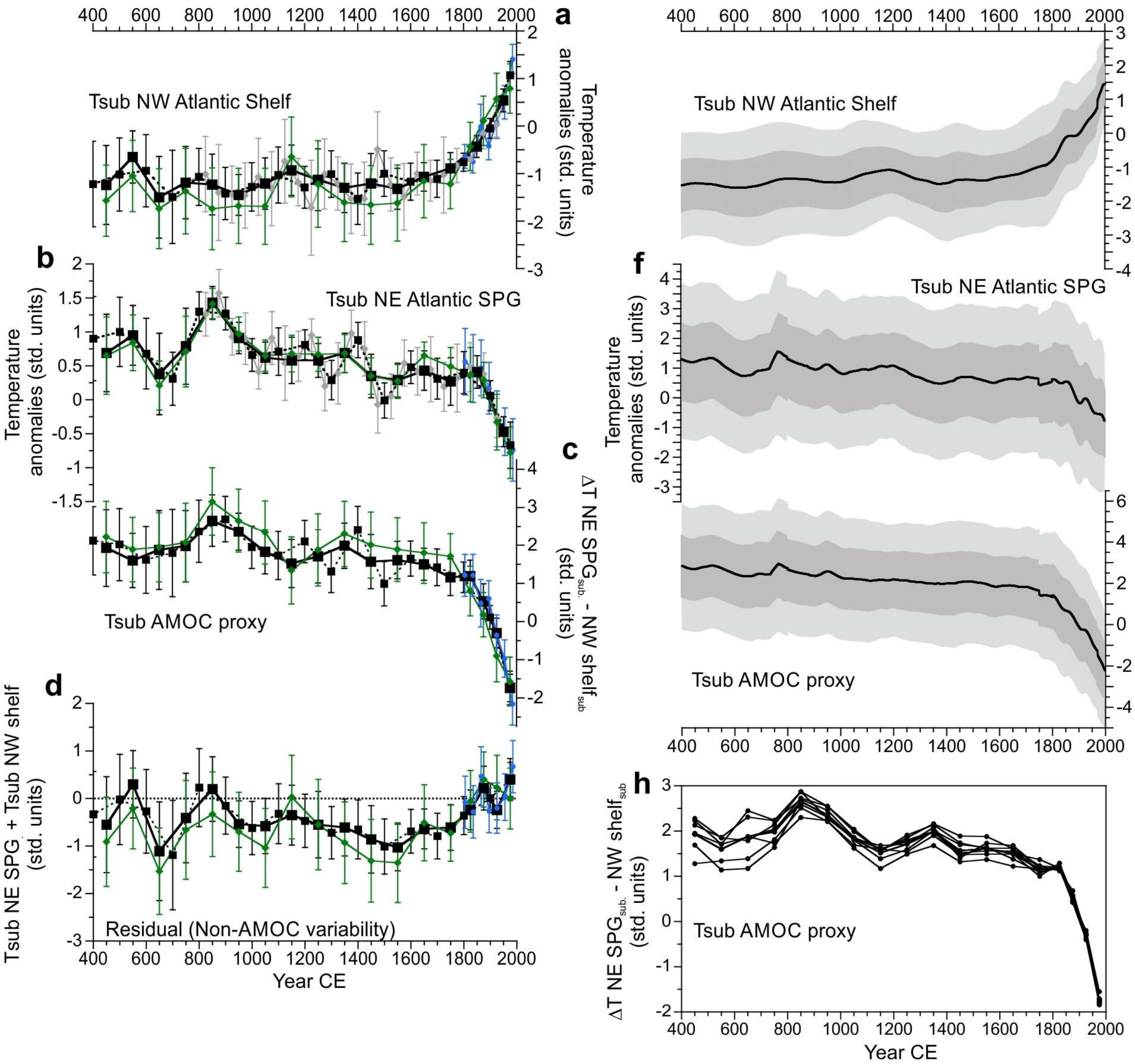

Extended Data Figure 4. Different binning and averaging approaches and the residual temperature signal. **a & b,** Stacked, normalized proxy temperature data from the NW Atlantic shelf/slope (**a**) and NE Atlantic SPG (**b**). **c,** The derived Tsub AMOC proxy calculated as the numerical difference between the stacks shown in **a** and **b**. **d,** The residual temperature variability in stacks **a** and **b** not described by the (anti-phased dipole) Tsub AMOC proxy shown in **c**, i.e. the in-phase temperature variability common to both stacks, calculated as the numerical sum of the two stacks (if divided by two, this would be the numerical mean). This represents the inferred non-AMOC related temperature variability common to both regions, and broadly resembles northern hemisphere temperature reconstructions, most notably colder residual temperatures during the LIA, ~1350-1850. For plots **a-d**: black solid line and squares, preferred binning (50yr for 1800-2000, 100yr for 400-1800); green line and symbols, as for preferred binning but stacks are produced by first binning the proxy data at each site and then averaging these binned site values, as opposed to binning all the proxy data together in one step (the former ensures equal weighting for each site, the latter biases the final result to the higher resolution records); black dashed line and symbols, 100yr bins offset by 50yr from the preferred bins; grey line and symbols, 50yr bins (not shown for **c** and **d**); blue line and symbols; 30yr bins for 1790-2000. Error bars for **a-d** are ±2S.E. **e-g,** as for **a-c** except using a Monte Carlo approach, using the published uncertainties for age assignment and temperature reconstructions; light and dark grey shading are $\pm 1\sigma$ and $\pm 2\sigma$. **h,** Jacknife approach version of **c**, with each line representing the Tsub AMOC proxy but leaving out one of the individual proxy records each time.

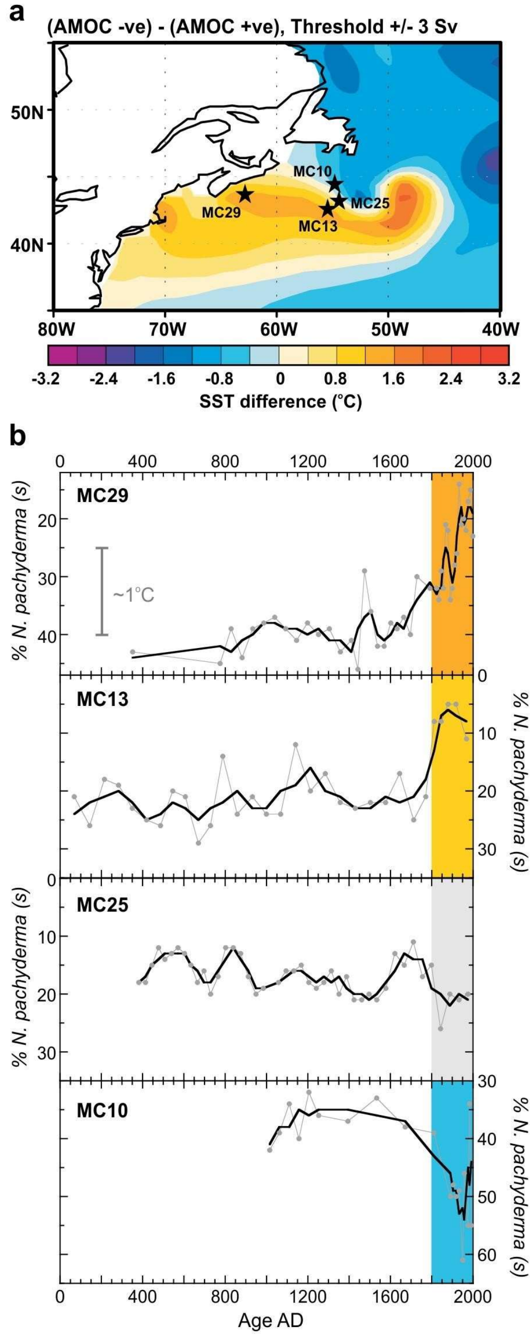

Extended Data Figure 5. SST temperature response of the Northwest Atlantic to AMOC weakening. a, Modelled SST difference between weak and strong AMOC[58]. This pattern is model-dependent, with the study cited here chosen because of its good agreement with observations of Gulf Stream variability[58]. Core locations for **b** are shown by black stars. **b,** The percentage abundance of the polar species, *N. pachyderma* (sinistral), in marine sediment cores from the Northwest Atlantic, as an indicator of near-surface (~75m) temperatures: a 15% increase indicates ~ 1°C of cooling (note the reversed y-axes). The opposing trends over the last 200 years are consistent with the modelled SST pattern for a weakening of the AMOC, as shown in **a**. Data and age models for the cores are: OCE326-MC29, ref.[48], using the original ^{14}C dating and as shown in Extended Data Fig. 2; OCE326-MC13 and OCE326-MC25, ref.[49], using the original ^{14}C age ties at the top and bottom of the core and scaling the intervening sedimentation rate to the %$CaCO_3$ content[49,59,60]; KNR158-MC10 from this study and age model presented in Extended Data Fig. 2.

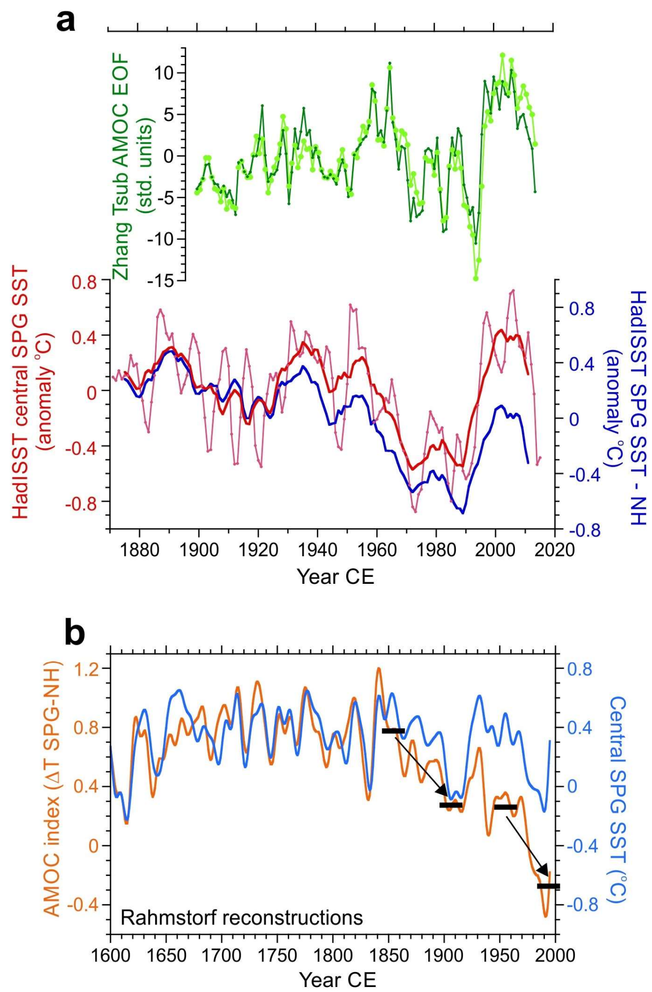

Extended Data Figure 6. Temperature fingerprints of AMOC over the twentieth century. a, Top, the Tsub AMOC fingerprint[11] using the EN4 dataset (light green is EOF1 of 1993-2003, as defined by Zhang[11], applied to the EN4 data; dark green is the 2nd EOF of the North Atlantic) - no 20th century AMOC decline is shown by this observational based reconstruction; bottom, instrumental based reanalysis of the 'cold blob' central SPG region (red, 3 yr and 11 yr smooth; 47-57N, 30-45W) used in the Rahmstorf SST AMOC proxy[6]. The reconstructed central SPG SST bears some resemblance to the Tsub AMOC fingerprint record, which is not unexpected since the central SPG forms a significant spatial component of the Tsub fingerprint. No clear decrease is shown by the central SPG SST, and the equivalent Rahmstorf AMOC proxy[6] (blue; central SPG – northern hemisphere (NH) temperature) declines through the twentieth century only due to the subtraction of the NH warming trend. **b,** Reconstructed (predominantly terrestrial-based proxy network) AMOC proxy (temperature difference between the central SPG and the NH; orange) and the central SPG SST reconstruction[6] (blue). As for the instrumental data shown in (**a**), the decline in the Rahmstorf AMOC index throughout the twentieth century is caused by the subtraction of the NH warming trend. There is a two-step decline in the AMOC proxy, at 1850-1900 and 1950-2000, the former mainly being the result of a strong cooling of the SPG (likely weakening northward heat transport, paralleling the weakening shown by our DWBC proxy), whereas the late twentieth century decline was mainly due to the subtraction of the strong NH warming trend, rather than a persistent cooling of the SPG.

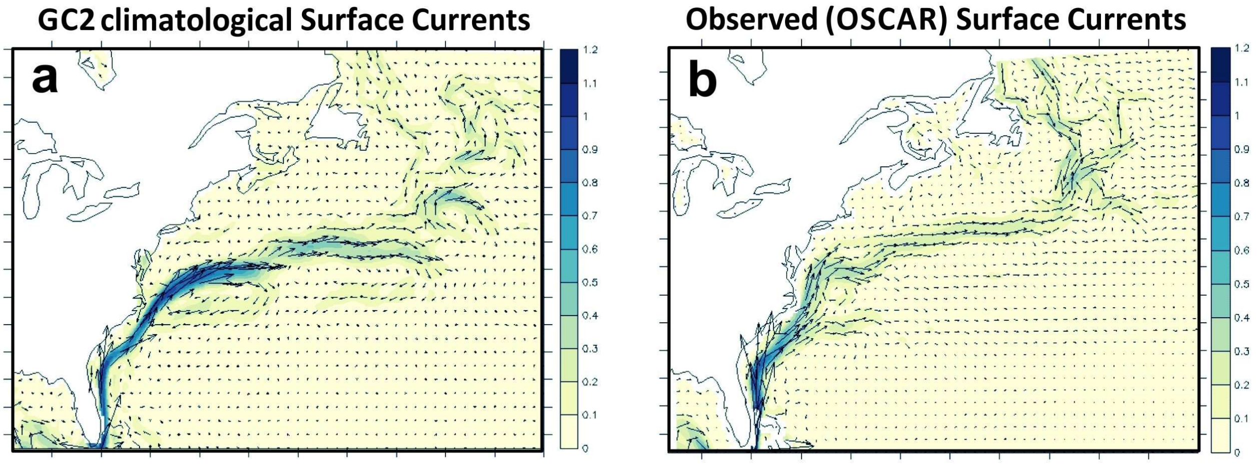

Extended Data Figure 7. DWBC changes in model HadGEM3-GC2. a,b Climatological surface current direction (in arrows) and speed (shaded, m/s) in the control simulation with HadGEM3-GC2 and the satellite product OSCAR, respectively.

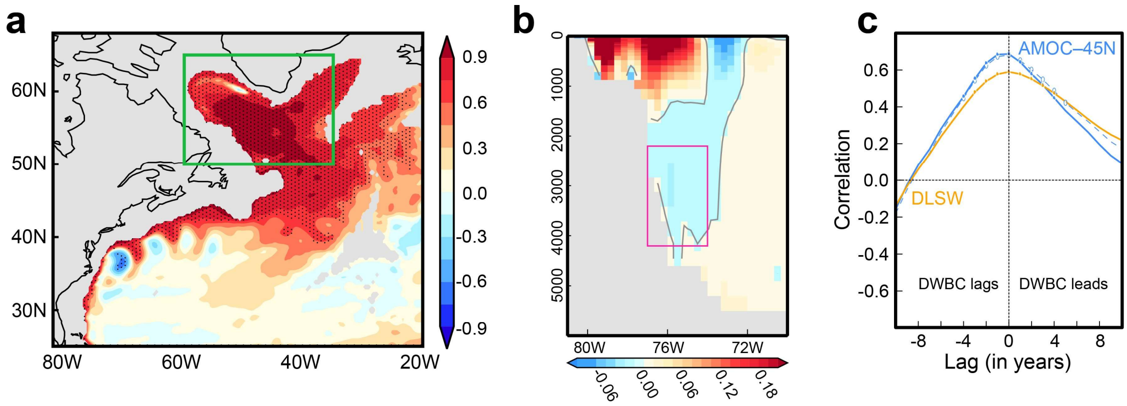

Extended Data Figure 8. The modelled link of DWBC velocity with deep Labrador Sea density and AMOC in the HiGEM model. a, Correlation of the vertically-averaged ocean density (1000-2500m) with deep Labrador Sea density index (dLSD as defined by ref. 4; green box, 1000-2500m average) in a 340 year present day control run of the HiGEM model (see ref 36). **b**, Climatology of the modelled meridional ocean velocity (ms^{-1}) averaged between 30-35ºN, illustrating the modelled position of the DWBC **c**, Cross-correlations between modelled averaged DWBC flow speed in pink box in **b** and indices of dLSD and AMOC at 45ºN (dashed line is without the Ekman component). Note that the box over which the DWBC flow index in **c** is averaged has changed with respect to Fig. 1 in the main paper in order to take into account of the fact that the return flow is deeper in HiGEM than in HadGEM3-GC2.

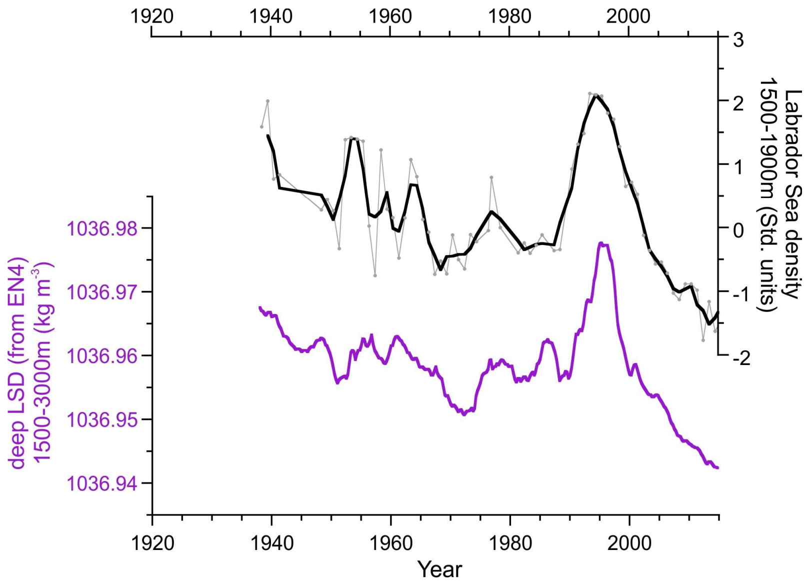

Extended Data Figure 9. Comparison of Labrador Sea density parameters. The model-based deep Labrador Sea density (dLSD) parameter, proposed by ref. 4, using the EN4 reanalysis dataset, incorporates a larger area and greater depth range than instrumental data-only studies such as ref. 5, which examines past variability in Labrador Sea convection and focuses on the central Labrador Sea and depths <2000m region, where most observational data is available. The comparison, here, of dLSD (purple line, 3 yr mean) using the EN4 dataset with instrumental data of density changes in the central Labrador Sea at 1500-1900m depth (black line, annual averages and 3 yr mean) illustrates that the two parameters show very similar variability, both being dominated by the density changes caused by deep convection in the Labrador Sea, which can reach down to ~2000m. Estimates of uncertainty are discussed in ref. [61].

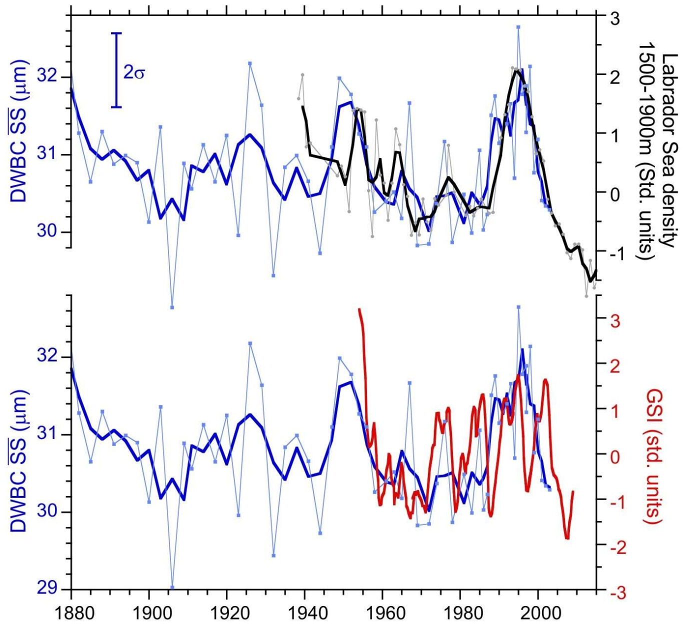

Extended Data Figure 10. Comparison with Gulf Stream Index (GSI). The direct influence of the changing position of the Gulf Stream on the grain size of our core sites can be ruled out through comparison of instrumental records of the Gulf Stream position (the GSI, from ref. [58]) with the down-core data in 56JPC. No clear correlation is observed between the GSI and our SS mean grain size data in core 56JPC, contrasting with the coupling between our SS data (inferred $DWBC_{LSW}$ flow speed) and density changes in the deep Labrador Sea. 2σ SS error bar (n=30) is for 3-point mean (bold).